Article

Optimizing of Culture Conditions for the Isolation and Characterization of Extracellular Vesicles Derived from Lactobacillus crispatus PMC201

Soyeon Lee , Youngkyoung Lee , Dongsic Choi , Haekang Yang , Hoonhee Seo , Ho-Yeon Song *

Posted Date: 13 May 2024

doi: 10.20944/preprints202405.0897.v1

Keywords: Extracellular vesicles; Lactobacillus crispatus PMC201; Probiotics; Proteome; Microbiome

 doi:10.20944/preprints202405.0897.v1

Article

Optimizing of Culture Conditions for the Isolation and Characterization of Extracellular Vesicles Derived from *Lactobacillus crispatus* PMC201

Soyeon Lee [1], Youngkyoung Lee [1], Dongsic Choi [2], Haekang Yang [2], Hoonhee Seo [1,3] and Ho-Yeon Song [1,3,*]

[1] Department of Microbiology and Immunology, School of Medicine, Soonchunhyang University, Cheonan, Chungnam, 31151, Korea
[2] Department of Biochemistry, Soonchunhyang University, Cheonan, Chungnam, 31151, Korea
[3] Human Microbiome Medical Research Center, Soonchunhyang University, Asan, Chungnam, 31538, Korea
* Correspondence: songmic@sch.ac.kr; Tel.: 041-570-2412

Abstract: Extracellular vesicles (EVs) carry diverse cargo of DNA, RNA, proteins, and lipids. They are crucial mediators for regulating various functions through interactions with the host. Recent investigations suggest that EVs or their constituent proteins derived from probiotics could improve the effectiveness of probiotic strains in disease management compared to probiotic strains themselves. This enhanced effectiveness arises from their innate antimicrobial properties, which can specifically target pathogenic molecules or cells, in addition to their significant ability to regulate immune responses. Significantly, previous studies have highlighted the inhibitory potential of *Lactobacillus crispatus* PMC201 against *Mycobacterium tuberculosis*. In this study, we focused on optimizing isolation conditions for studying extracellular vesicles and proteins from anti-TB potent strains. We provide analysis results based on food-grade media (FGM) optimization and isolation methods. Nanoparticle tracking analysis (NTA) was used to determine secretion patterns. Proteomic analysis was performed by liquid chromatography and tandem mass spectrometry (LC-MS/MS). A total of 64 proteins were identified in the *L. crispatus* PMC201 strain, particularly enriched in s-layer and splX. Questions remain about their relevance to anti-TB. This anti-tuber strain has potential as a therapeutic agent, given its significant role in intercellular killing. Further studies are needed to investigate its mechanisms of action.

Keywords: extracellular vesicles; *Lactobacillus crispatus* PMC201; probiotics; proteome; microbiome

1. Introduction

According to the World Health Organization (WHO) and the U.S. Food and Administration (FDA), probiotics are microorganisms that are beneficial to the health of the host when consumed in sufficient quantities [1] and food ingredients that can increase the intake of beneficial microorganisms in the human body when consumed [2]. Probiotics are microorganisms that are beneficial to the host. They are commonly found in the digestive tract, where they live in symbiosis with humans. They are subjects of much microbiome research. Probiotics are known to benefit human health and play a particularly significant role in supporting good health [3]. They hold significant potential in mitigating conditions associated with dysbiosis, including allergic disorders, gastrointestinal diseases, metabolic ailments, oncological conditions, and cardiovascular pathologies [4]. Probiotics produce a wide range of bioactive compounds including vitamins, short-chain fatty acids (SCFAs), amino acids, peptides, enzymes, and exopolysaccharides (EPS) that can promote beneficial health effects for the host [5]. Particularly, lactic acid bacteria (LAB) celebrated for their ability to produce Gram-positive lactate have been categorically presented as probiotic frontrunners [6]. Probiotics play a significant role in enhancing host defenses against infections through diverse mechanisms [7]. They

 doi:10.20944/preprints202405.0897.v1

reinforce the epithelial barrier, inhibit pathogen adhesion, and competitively modulate colonization of pathogenic microbes. Additionally, probiotics can produce antimicrobial agents, modify toxins, and boost host immune responses through both nonspecific and specific immune stimulation [8]. However, understanding specific pathways and regulatory molecules responsible for beneficial effects of probiotics remains challenging [9]. Significant progress has been made in chemistry, biology, and membrane vesicle research over the past decade. These advancements have enhanced the efficiency and targeted delivery of probiotics, expanding their utility in treating various diseases [10]. Recent investigations have emphasized the significance of EVs derived from probiotics and indicated their significant role in enhancing probiotic efficacy [11,12]. EVs play essential roles in interactions between bacteria and hosts, transporting signals associated with immune responses and modulating diverse signaling pathways [13]. Protein compositions of bacteria-derived extracellular vesicles (BEVs) vary depending on specific attributes such as taxonomic categorizations (genus, species, lineage) and symbiotic or pathogenic characteristics. BEVs appear as spherical or nano-sized vesicles, with diameters ranging from 20 nm to 400 nm. They transport abundant microRNAs, mRNAs, proteins, and assorted bioactive factors [14,15]. BEVs primarily activate immune cells. In microbial communities, bacterial cells engage in complex interactions, wherein EVs play significant roles in both cooperative and competitive strategies [16]. Several studies have reported that bacterial EVs can mediate resistance through various mechanisms, including horizontal gene transfer [17], representation of extracellular and intracellular antibiotics by EVs, and presence of enzymes for antibiotic resistance associated with EVs. BEVs can bind/capture antibiotics in the extracellular compartment, thereby protecting microbial communities and providing bacteria with defense against various antibiotics. EVs represent a set of microbial-associated molecular patterns (MAMPs) recognized by specific receptors expressed in epithelial and immune cells of the host [18]. These pattern recognition receptors (PRRs) are considered vital components of innate immunity as they can detect intestinal microbes and mediate appropriate immune responses [19]. Toll-like receptors (TLRs) primarily located on the cell surface or within endosomal membranes can initiate cellular signaling pathways that regulate immune and defensive responses when they bind to MAMPs such as polysaccharides, lipopolysaccharides (LPS), and lipoproteins found on surfaces of EVs. These attributes suggest the involvement of vesicles in the interplay between infection and the immune system [20,21]. Previous studies have reported that two *Lactobacillus* strains, *L. crispatus* and *L. gasseri*, isolated from vaginal microbiota of healthy women, can release EVs to protect human cells and tissues from HIV-1 infection. These EVs contain various bacterial metabolites and proteins associated with anti-HIV-1 effects [22]. Moreover, EVs can directly deliver therapeutic substances, supporting targeted action on specific molecules or cells. This can enhance treatment efficiency and precision compared to using microbial strains alone as therapeutics. Previous studies have confirmed the effectiveness of *Lactobacillus crispatus* PMC201 in reducing *M. tuberculosis* H37Rv and extensively drug-resistant (XDR) *M. tuberculosis* in co-culture conditions [23]. This study was conducted to find optimal conditions for studying probiotic derived EVs. In addition, the corresponding proteome was confirmed. For *L. crispatus* PMC201, EVs were isolated using food-grade medium [24], a self-developed medium rather than commercial media. Proteomic analysis was then performed using liquid chromatography coupled with tandem mass spectrometry (LC-MS/MS) [25,26]. In *L. crispatus* PMC201, a total of 64 proteins were identified, predominantly composed of cell wall constituents.

2. Materials and Methods

2.1. Optimized Culture Media for Isolating of EVs

Food-grade culture medium, a self-made medium rather than a commercial one, was prepared by adding 10 g of Soy Peptone A2 SC, 10 g of yeast extract, 20 g of glucose, 1 ml of Tween 80, 0.1 g of magnesium sulfate, and 5 g of sodium chloride to 1 L of water

 doi:10.20944/preprints202405.0897.v1

2.2. Isolation of Bacterial EVs

L. crispatus PMC201 was cultured in a food-grade medium at 37°C on a shaking incubator (Biofree, Seoul, KOR) for 20 hours. Subsequently, the optical density (OD) of the probiotic culture was confirmed to be in the range of 1.0–1.2 using a portable VIS spectrophotometer (DR 1900, Hatch) at 600 nm. *L. crispatus* PMC201 was pelleted by centrifugation twice at 3515 × g for 20 minutes at 4°C. The culture supernatant of *L. crispatus* PMC201 was filtered through a 0.22 μm membrane (Merck Millipore, Burlington, MA, USA) and concentrated 10-fold using a 100-kDa membrane filter (Pall, Port Washington, NY, USA). It was further concentrated 10-fold with an Amicon Ultra Centrifugal Filter (100 kDa MWCO). EVs derived from *L. crispatus* PMC201 were purified from culture supernatants concentrated 100-fold. For the ultracentrifugation (UC) method, the concentrated conditioned medium was centrifuged at 150,000 g for 2 hours at 4°C using an ultracentrifuge Optima MAX-XP (Beckman Coulter, Fullerton, CA, USA) with an MLA-55 rotor. Pelleted EVs were resuspended in PBS. Size exclusion chromatography (SEC) method obtains fractions using a qEVoriginal/35 nm Gen 2 column (Izon Science, Christchurch, NZ). Protein content was quantified using a Micro BCA assay (Thermo Scientific, 23235).

2.3. Bio-TEM Imaging of EVs

To visualize EVs samples, transmission electron microscopy (TEM) was utilized. For negative staining, EVs samples were affixed to a carbon-coated 200-mesh copper grid and then stained with 2% (w/v) uranyl acetate. Imaging of EVs was performed using a 120 kV TEM (Bio-TEM, Tecnai G2 Spiri TWIN, FEI). Diameters of EVs were determined using ImageJ software, with measurements obtained at 200 nm through a CCD camera.

2.4. NTA Measurements of EVs

Size distribution analysis and concentration measurements were performed using the nanoparticle tracking analysis (NTA) and Nano Sight NS300 system with a sCMOS camera, Green488 laser, and NTA software Version 3.4 (Malvern Instruments, Malvern, UK). Before analysis, samples were vortexed and diluted to 1 mL with PBS buffer. Measurements were performed at 25°C. Samples were recorded three times for 60 s with a camera level of 16 and the threshold parameter set at 5 to obtain concentrations in the range of 10^7–10^9 particles mL−1 (corresponding to 20–100 particles per frame).

2.5. Methanol/Chloroform Precipitation

Proteins were precipitated using a methanol/chloroform mixture to remove lipids. A 100 μg protein sample was mixed with methanol (260 μL) and vortexed. After centrifugation at 9,000 x g for 10 seconds, chloroform (65 μL) was added and the mixture was vortexed and centrifuged again. After adding HPLC-grade water (195 μL), the solution was centrifuged at 16,000 x g for 2 minutes to pellet proteins. Methanol (195 μL) was then added to the protein pellet, vortexed, and centrifuged at 16,000 x g for 3 minutes. The supernatant was removed and the protein pellet was air-dried before resuspension in 30 μL of 2X dye for further analysis.

2.6. SDS-PAGE and Coomassie Blue Staining

SDS-PAGE was conducted to separate proteins based on molecular weight. Equal numbers of purified EVs derived from *L. crispatus* PMC201 were analyzed using denaturing polyacrylamide gel electrophoresis with a linear concentration gradient of polymer (4–15% Tris-glycine gel). Following electrophoresis at 150 V for 70 min, the gel was then stained with Gel Code Blue Stain Reagent (Thermo, USA), destained, and imaged using a Bio-Rad ChemiDoc MP Imaging System

 doi:10.20944/preprints202405.0897.v1

2.7. Proteomic Analysis of EVs Derived from L. crispatus PMC 201

All analyses were performed in triplicate to ensure reliability. A total of 200 μg of EVs underwent methanol/chloroform precipitation according to the established protocol (PMID: 33420990). Precipitated proteins were subsequently subjected to in-gel digestion by trypsin following procedures outlined in a previous study (PMID: 34200450). Resulting tryptic peptides were dissolved in 20 μL of buffer A (0.1% formic acid in water) and 5 μL was injected onto a trap column, Acclaim PepMap C18 nano Viper 100 (75 μm × 2 cm, 3 μm) (Thermo Fisher Scientific) with a flow rate of 5 μL/min using 95% buffer A for 4 min for LC-MS/MS analysis. This analysis was performed using an Orbitrap Eclipse™ Tribrid™ mass spectrometer (Thermo Fisher Scientific, San Jose, USA) coupled with an Ultimate™ 3000 UHPLC system (Thermo Fisher Scientific, USA). Peptides were separated on an analytical column, PepMap RSLC C18 ES803A (75 μm × 50 cm, 2 μm) (Thermo Fisher Scientific), using a 180 min gradient with 5-90% of solvent B (0.1% formic acid in acetonitrile) at a flow rate of 300 mL/min. The mass spectrometer was operated in a data-dependent Top 20 scans mode, switching between MS and MS2. Peptides were analyzed with the following parameters: 10 ppm of mass accuracy, 1850 V of ion spray voltage, 275°C of capillary temperature, m/z 375-1575 resolution for full scans, and 120,000 higher-energy collisional dissociation activation scans with 35% normalized collision energy. The quadrupole isolation window was set to 1.4 Da. MS/MS spectra were detected using an Orbitrap instrument with a resolution of 30,000. MS raw files were analyzed using the MaxQuant program (version 2.2.0.0) (Max Planck Institute, Germany) against the *L. crispatus* PMC201 protein database (release 2023_04) from UniProt. A tolerance of 20 ppm was applied for precursor ions and fragment ions. Trypsin digestion allowed for up to two potential missed cleavages. Modifications included fixed carbamidomethylation of cysteine (57 Da) and variable deamidation of asparagine and glutamine (1 Da), methionine oxidation (16 Da), and N-terminal acetylation (42 Da). All identified proteins underwent statistical processing using the Scaffold program (version 5.3.0). Proteins meeting a protein threshold of ≥ 0.95 and containing a minimum of 2 peptides with a protein threshold of ≥ 0.95 were selected for further analysis. Protein quantitation was conducted using normalized weighted spectra in the Scaffold program.

2.8. Integrated Bioinformatics Analysis of protein Sequences from Proteomic Data

Protein bioinformatics analysis was conducted using a subset of data obtained through the Scaffold program (version 5.3.0) for proteomic analysis. Identified protein sequences were analyzed through protein-protein interaction network analysis using String (version 12.0). Protein network visualization used Cytoscape (version 3.8.2). Protein location prediction used DeepLoc2. Subsequently, sequences were mapped to Gene Ontology (AmiGO 2) to verify their biological and functional properties. Furthermore, enriched pathways associated with identified proteins were evaluated using the Kyoto Encyclopedia of Genes and Genomes (KEGG) database. Data were visualized using R programming. Data were visualized using R programming.

2.9. Statistical Analysis

NTA data used GraphPad Prism(version.10) software to conduct the statistical analysis, specifically using the t-tests (p-value < 0.05 or 0.01). Statistical significance was considered for P-values (P) of ≤0.05. Protein pathways data values were based on intensity values derived from network analyses (PPI enrichment p-value $<1.0\times10^{-16}$, FDR ≤ 0.05).

3. Results

3.1. Isolation of EVs Derived from L. crispatus PMC201

EVs were isolated by removing bacterial pellets and cell fragments, EVs were filtered and concentrated using a 100 kDa cutoff to prevent the presence of EVs with molecular weights < 100 kDa in the supernatant. Finally, EVs were pelletized through ultracentrifugation to remove supernatants and any remaining soluble proteins to isolate EVs (Figure 1A). Subsequently, we identified proteins

 doi:10.20944/preprints202405.0897.v1

secreted by these EVs. To isolate EVs, SEC and UC methods were employed. The presence of EVs in the isolated sample was confirmed through TEM and NTA. Both SEC and UC verified that *L. crispatus* PMC201 secreted EVs.

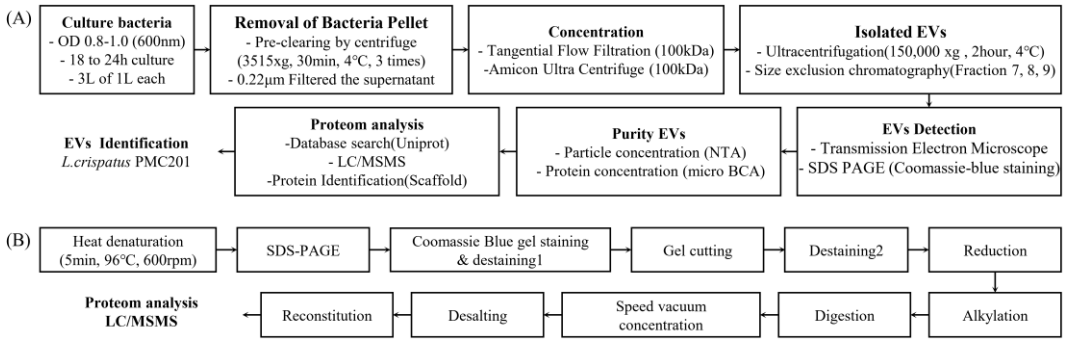

Figure 1. Workflow design for isolation and proteome analysis of extracellular vesicles (EVs) derived from *L. crispatus* PMC201. (A) Workflow for isolating EVs for proteomic analysis involved several key steps. Initially, ultracentrifugation was employed as the fundamental method for performing proteomic analysis of EVs. Recently, size exclusion chromatography has appeared as an alternative method for isolating EVs. The detection of EVs is crucial to confirm their presence and assess their purity, ensuring cleaner samples for subsequent proteomic analysis. (B) Protein digestion methods for proteomic analysis.

3.2. Comparison of EVs Size and Concentration

3.2.1. Comparison of EVs between Culture Media

EVs isolated from *L. crispatus* PMC201 were obtained using the SEC method under two culture conditions using MRS media or food-grade media. SEC yielded fractions 7 and 8, which were typically associated with EVs. To quantify nanoparticles in EVs obtained from both culture media, NTA was employed (Figure 2, Table 2). Although the size of *L. crispatus* PMC201 was confirmed to be larger in MRS media than in food-grade media, the particle number was measured to be higher for *L. crispatus* PMC201 grown in food-grade media. Since this was a result obtained by diluting 10 times, when total particles were checked, it was confirmed that EVs obtained by culturing *L. crispatus* PMC201 in food-grade media secreted 2.5 times more particles. Sizes of EVs obtained from both media were in the range of 30 nm to 200 nm. However, since food-grade media clearly secreted a large amount of EVs at this concentration, it is efficient to isolated EVs by culturing *L. crispatus* PMC201 in food-grade media (Table 1) [PMC 201- MRS: (Mean: 136+/-7.1 nm, Mode: 107.6+/-8.7 nm, SD: 62.3+/-12.6 nm, Concentration (particles/mL): 1.06×10^{7}+/-9.60×10^{6}), PMC 201-FGM: (Mean: 119.8+/-5.3 nm, mode: 88.05+/- 6.7 nm, SD: 58.6+/-12.1 nm, concentration (particles/mL): 2.31×10^{8}+/ -1.02×10^{7})]

Table 1. Food-grade media composition.

Ingredient's name	Commercial name of ingredients	Number of Hits
Soy peptone A2 SC	Soy peptone A2 SC	10g
Yeast extract	Amberferm	10g
Glucose	Dextrose	20g
Tween 80	Tween 80	1ml
Magnesium sulfate	Magnesium sulfate	0.1g
Sodium chloride	Sodium chloride	5g

 doi:10.20944/preprints202405.0897.v1

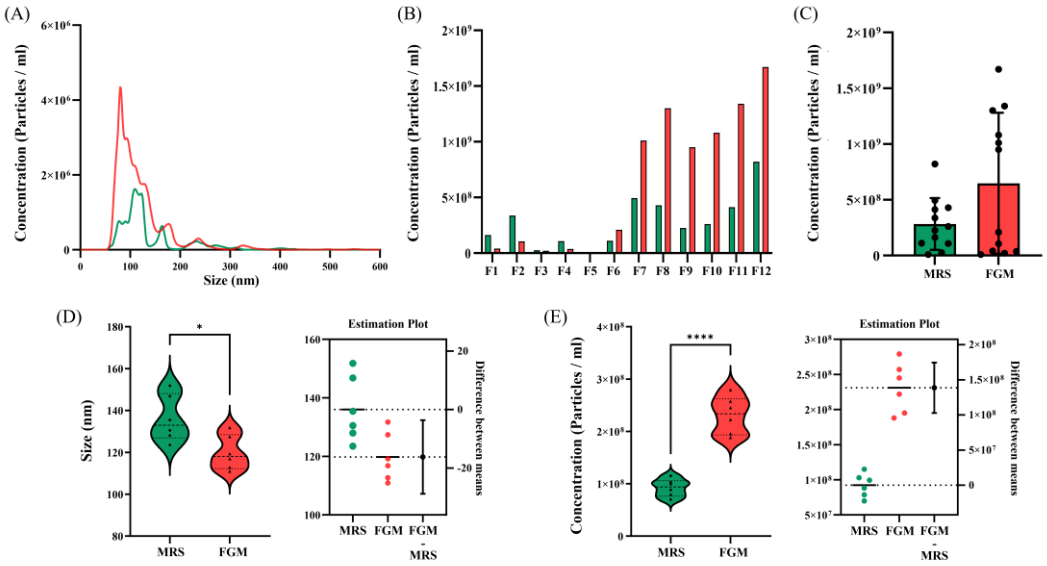

Figure 2. Differences in particle count of extracellular vesicles (EVs) depending on culture media. (A) Nanoparticle tracking analysis (NTA) signals of extracellular vesicles according to culture media. Mean particle counts secreted after culturing in MRS media and food-grade media (FGM). (B), (C) Particle counts and distribution of fractions separated by size exclusion chromatography (SEC). Comparison of (D) size and (E) concentration distribution.

Table 2. Concentration and size of nanoparticles, enriched by Culture media and isolation method as measured by NTA.

Culture media / Isolation method	MRS / SEC	FGM / SEC	FGM / UC
Mean	136+/-7.1 nm	119.8+/-5.3nm	166.9+/-13.5 nm
Mode	107.6+/-8.7 nm	88.05+/-6.7 nm	110.1+/-7.0 nm
SD	62.3+/-12.6 nm	58.6+/-12.1 nm	89.9+/-4.1 nm
Concentration(particles/mL)	1.06×10^{7}+/-9.60×10^{6}	2.31×10^{8}+/-1.02×10^{7}	3.50×10^{8}+/-2.54×10^{7}

3.2.2. Comparison of EVs According to Isolation Methods

EVs isolated from *L. crispatus* PMC201 was obtained using SEC and UC methods (Figure 1A). Since previous results showed that particle secretion was more prominent in food-grade media than in MRS, EVs were isolated from strains grown in food-grade media for both SEC and UC. Fractions 1-12 of SEC were identified, yielding fractions 7 and 8, which were generally associated with EVs (Figure 3B). To quantify nanoparticles in EVs obtained from both concentration methods, NTA was employed (Figure 3, Table 2). For PMC 201, the number of nanoparticles was similar with both SEC and UC. However, the size was significantly larger in UC than in SEC [PMC 201 - SEC: (Mean: 119.8+/-5.3 nm, Mode: 88.05+/-6.7 nm, SD: 58.6+/-12.1 nm, Concentration (particles/mL): 2.31×10^{8}+/-1.02×10^{7}), PMC 201 - UC: (Mean: 166.9+/-13.5 nm, Mode: 110.1+/-7.0 nm, SD: 89.9+/-4.1 nm, Concentration (particles/mL) : 3.50×10^{8}+/-2.54×10^{7})](Figure 3A). As a result of comparing EVs isolated from *L. crispatus* PMC201 separated in SEC and UC, both size and particle number were observed to be higher in UC than in SEC (Figs. 3C, D). In the case of particle number, those in UC secreted 1.5 times more particles than those in SEC. This suggests that it is more efficient to isolate EVs using UC than using SEC.

 doi:10.20944/preprints202405.0897.v1

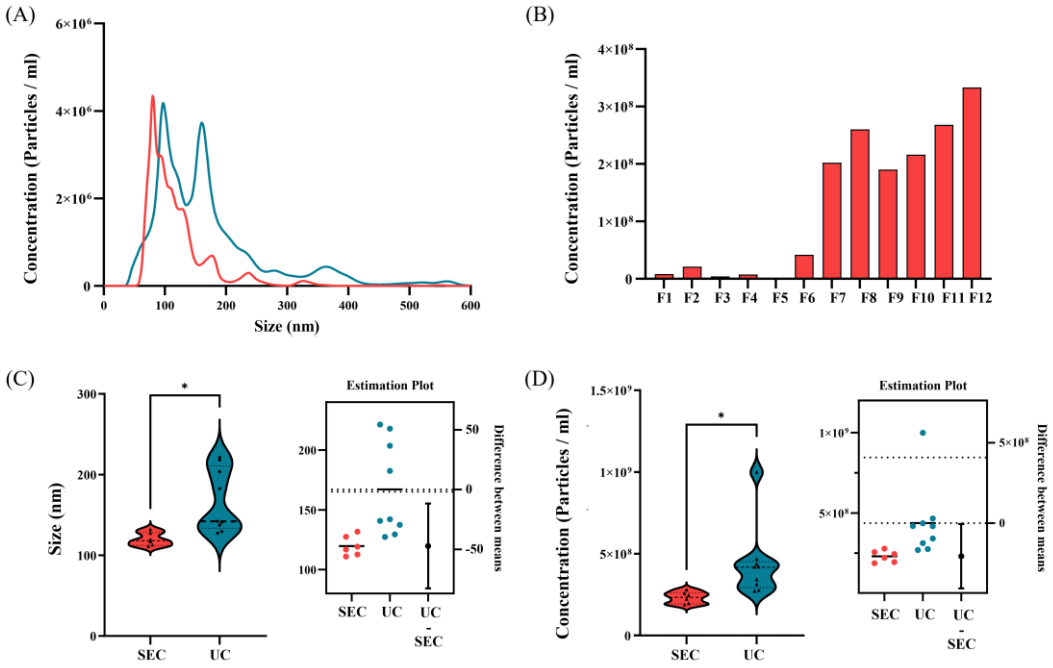

Figure 3. Difference in number of extracellular vesicles (EVs) particles depending on isolation methods. (A) Nanoparticle tracking analysis (NTA) signals for EVs derived from *L. crispatus* PMC 201 obtained from size exclusion chromatography (SEC) and ultracentrifugation (UC) samples. (B) Concentration distribution of EVs derived from *L. crispatus* PMC 201 SEC fraction. Comparison of (C) size and (D) concentration distribution between EVs derived from *L. crispatus* PMC 201.

3.3. EVs Derived from L. crispatus PMC201 Confirmed by TEM

Shapes of EVs isolated from *L. crispatus* PMC201 were confirmed by TEM. Imaging confirmed the presence of EVs derived from *L. crispatus* PMC201 within the size range of 100-200 nm (Figure 4). Previously, measuring the size using NTA (Figure 3) revealed that nanoparticles of all samples had sizes in a range of 100 nm to 200 nm. Samples isolated by UC showed a spectrum of cup-shaped extracellular vesicles of diverse sizes and shapes (Figure 4A). In contrast, samples isolated with SEC had fewer impurities, although they had a smaller number of EVs compared to those isolated with UC (Figure 4B). Specifically, EVs derived from *L. crispatus* PMC 201 exhibited a relatively high purity with comparatively uniform shape and size distribution.

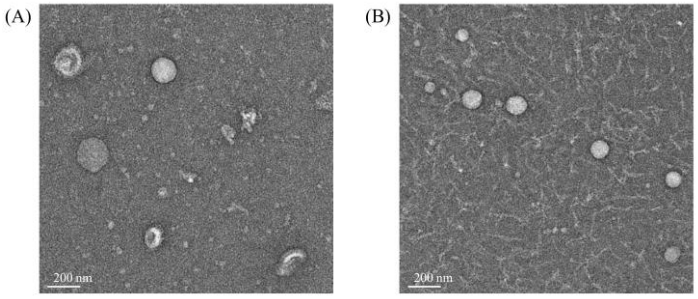

Figure 4. Extracellular vesicles (EVs) derived from *L. crispatus* PMC201 confirmed by a transmission electron microscopy (TEM). Transmission electron microscopy (TEM) imaging confirmed the presence of EVs derived from *L. crispatus* PMC201 with sizes in a range of 200 nm. (A) EVs derived from *L. crispatus* PMC 201 isolated by ultrafugation (UC). (B) EVs derived from *L. crispatus* PMC 201 samples isolated by size exclusion chromatography (SEC).

 doi:10.20944/preprints202405.0897.v1

3.4. Proteome Profiling of EVs Derived from L. crispatus PMC201

3.4.1. LC-MS/MS Analysis

To identify proteins secreted by EVs derived from *L. crispatus* PMC201, isolated EV samples (n = 3) were digested in a solution and analyzed using LC-MS/MS with an Orbitrap Eclipse TM Tribrid TM mass spectrometer (Thermo Fisher Scientific, San Jose, CA, USA) coupled with an Ultimate TM 3000 UHPLC system (Thermo Fisher Scientific, USA). All identified proteins were statistically processed using the Scaffold program (version 5.3.0) (Figure 1B). Only proteins with a protein threshold ≥ 0.95 and one minimum peptide of two were selected for further analyses. Under these conditions, 64 proteins were identified in EVs derived from *L. crispatus* PMC201 (Figure 5A). In EVs derived from *L. crispatus* PMC201, S-layer protein showed the highest abundance at 301 (Figure 5B). This proteomic study identified proteins in EVs derived from *L. crispatus* PMC201 (Table 3).

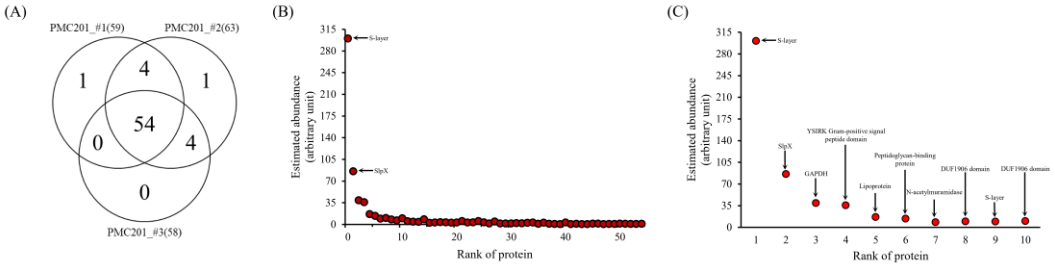

(D)

#	Gene symbol	Protein name	MW	Abundance
1	HMPREF9249_00107	S-layer protein	47 kDa	301
2	GTO85_09750	SlpX protein	53 kDa	86
3	gap	Glyceraldehyde-3-phosphate dehydrogenase	37 kDa	39.33
4	CEE75_13625	YSIRK Gram-positive signal peptide domain-containing protein	51 kDa	35.67
5	LBKG_00481	Lipoprotein	34 kDa	16.67
6	CEE75_08410	Peptidoglycan-binding protein	23 kDa	14
7	CEE75_01100	N-acetylmuramidase	45 kDa	8.33
8	AEL95_04650	DUF1906 domain-containing protein	44 kDa	9.67
9	ERD32_05220	S-layer protein	43 kDa	9.33
10	AEL95_02570	DUF1906 domain-containing protein	34 kDa	10.33

Figure 5. Proteomic analysis of extracellular vesicles (EVs) derived from *L. crispatus* PMC201. Proteomic analysis of EVs derived from *L. crispatus* PMC 201. (A) Venn diagram of numbers of proteins identified in EVs (technical replicate n = 3). A total of 64 proteins was identified from EVs. The distribution of estimated abundance of whole (B) and top 10 abundant (C) proteins in EVs according to their abundance ranks. (D) Top 10 abundant vesicular proteins according to their abundance ranks are listed with their gene symbols, protein names, molecular weight, and abundance. Classical EVs marker proteins are highlighted. (F) The protein size is verified through Coomassie blue staining, consistent with proteomic data.

Table 3. Identified proteins from extracellular vesicles (EVs) derived from *L. crispatus* PMC201.

Accession	Identified Proteins	Alternate ID	Molecular Weight
K1NK16	S-layer protein	HMPREF9249_00107	47 kDa
A0A6M1GK10	S-layer protein (Fragment)	G5T20_09495	44 kDa
A0A5M9Z605	S-layer protein	F1C07_06475	47 kDa
A0A854PP49	Surface layer protein A domain-containing protein	AYP82_00340	47 kDa
A0A5M9Z4Y9	S-layer protein OS=*Lactobacillus crispatus*	F1C07_06510	47 kDa
A0A854PLV2	Surface layer protein A domain-containing protein	AYP82_00370	47 kDa
A0A109DEN3	Surface layer protein A domain-containing protein	AEL95_05125	27 kDa
A0A109DCK1	S-layer protein (Fragment)	AEL95_10035	49 kDa
A0A135YNS0	Bacterial surface layer protein (Fragment)	HMPREF3209_02474	60 kDa
A0A7H9EBL4	SlpX protein	GTO85_09750	53 kDa

 doi:10.20944/preprints202405.0897.v1

A0A135YZ62	Bacterial surface layer protein	ERD32_09040	53 kDa
C7XGC7	Glyceraldehyde-3-phosphate dehydrogenase	gap	37 kDa
A0A4R6CPL7	YSIRK Gram-positive signal peptide domain-containing protein	CEE75_13625	51 kDa
E3R2H8	Lipoprotein	LBKG_00481	34 kDa
A0A4R6CS48	Peptidoglycan-binding protein	CEE75_08410	23 kDa
A0A4R6CWH5	N-acetylmuramidase	CEE75_01100	45 kDa
A0A109DEL0	DUF1906 domain-containing protein	AEL95_04650	44 kDa
A0A135Z2L1	S-layer protein	ERD32_05220	43 kDa
A0A109DTG6	DUF1906 domain-containing protein	AEL95_02570	34 kDa
A0A109DRM6	PDZ domain-containing protein	AEL95_06810	43 kDa
A0A109DF87	Cell division protein	AEL95_03480	63 kDa
A0A4R6CR16	Gram-positive cocci surface proteins LPxTG domain-containing protein (Fragment)	CEE75_10850	64 kDa
A0A109DF34	Surface layer protein A domain-containing protein	AEL95_03475	27 kDa
A0A120DIM9	Enolase	eno	47 kDa
A0A125P6L3	Uncharacterized protein	AEL95_00975	24 kDa
A0A109DWU7	Glucose-6-phosphate isomerase	pgi	49 kDa
A0A135ZEW6	HNH endonuclease	HMPREF3209_00721	35 kDa
A0A120DI73	DUF1002 domain-containing protein	AEL95_06965	34 kDa
A0A4Q0LXU7	Autotransporter	ERD32_01305	17 kDa
A0A4R6CRX5	Membrane transport protein MMPL domain-containing protein	CEE75_08755	124 kDa
D0DGZ7 (+2)	Uncharacterized protein	HMPREF0508_00896	23 kDa
D0DH00	Phage minor structural protein, N-terminal domain protein	HMPREF0508_00899	72 kDa
A0A135ZH00	Penicillin-binding protein, transpeptidase domain protein	HMPREF3209_00031	74 kDa
A0A135ZG11	Copper oxidase	ERD32_05870	59 kDa
A0A109DGH2	Hydrolase	AEL95_00120	32 kDa
A0A109DGC6	Glycosidase	AEL95_00130	20 kDa
A0A109DES4	Surface layer protein A domain-containing protein	AEL95_04840	27 kDa
A0A109DE36	Pyruvate oxidase	spxB	67 kDa
K1MKS9	DUF3383 family protein	HMPREF9249_02106	48 kDa
A0A109DCM5	Lysin	AEL95_09750	42 kDa
A0A109DME9	Large ribosomal subunit protein	rplF	19 kDa
A0A109DVU6	Phosphoglycerate kinase	pgk	43 kDa
A0A135Z6Y8	Dipeptidase	HMPREF3209_01335	53 kDa
A0A109DFB8	Extracellular solute-binding protein	AEL95_02275	44 kDa
A0A4V6PQ54	Phosphate-binding protein	CEE75_08510	31 kDa
A0A226V487	non-specific serine/threonine protein kinase	pknB	75 kDa
A0A120DIW3	Surface layer protein A domain-containing protein	AEL95_02090	46 kDa
A0A4Q0LY00	DUF2184 domain-containing protein	ERD32_01340	35 kDa
A0A109DIV5	Aggregation promoting factor	AEL95_07365	25 kDa
A0A125P6A1	Cell surface protein	AEL95_06085	42 kDa
A0A120DIL8	D-2-hydroxyacid dehydrogenase	AEL95_03565	38 kDa
A0A109DF57	Beta-lactamase family protein	AEL95_03595	39 kDa
A0A135ZB87	Signal peptide protein, YSIRK family	CEE75_00270	33 kDa
A0A109DGV4	Foldase protein PrsA	prsA	33 kDa
A0A2I1WJR8	Peptidase M13	CYJ80_03380	73 kDa

 doi:10.20944/preprints202405.0897.v1

A0A109DF15	L-lactate dehydrogenase	ldh	35 kDa
D0DH11	DUF3277 domain-containing protein	HMPREF0508_00910	14 kDa
A0A120DIB4	Bifunctional oligoribonuclease/PAP phosphatase NrnA	AEL95_05665	35 kDa
A0A109DJD1	PTS mannose family transporter subunit IID	AEL95_07920	34 kDa
A0A2N5KZX0	Bifunctional metallophosphatase/5'-nucleotidase	CYJ79_03285	91 kDa
A0A6M1GF03	Phage holin	G5T20_00725	14 kDa
A0A109DVJ8	Aggregation promoting factor surface protein	AEL95_07990	13 kDa
A0A135Z466	pullulanase	pulA	140 kDa
A0A109DPT6	DUF5052 domain-containing protein	AEL95_09755	23 kDa

3.4.2. Confirmation of Protein Sizes through Coomassie Blue Staining

Through Coomassie blue staining, we assessed protein sizes, revealing a range of sizes with several bands exhibiting distinct visibility. Notably, for EVs derived from *L. crispatus* PMC201, the most prominent band fell within the 42-49 kDa range (Figure 5F). LC/MS/MS analysis of proteomics data revealed that a 47 kDa S-layer protein was the most prominent band for EVs derived from *L. crispatus* PMC201 in terms of abundance (Figure 5C, D).

3.5. Prediction of Protein Pathways and Interaction of EVs Derived from L. crispatus PMC201

3.5.1. Cellular Components in Protein from EVs Derived from *L. crispatus* PMC201

Analysis of EVs derived from *L. crispatus* PMC201 identified distinct cellular components, including the extracellular region, peptidoglycan-based cell wall, cell wall, and S-layer with strength (Log10(observed / expected)) values ranging from 0.91 to 1.47, indicating moderate to high enrichment effects. Corresponding false discovery rates ranged from 0.0014 to 0.0145 (Table 4).

Table 4. Cellular Component of proteins from extracellular vesicles (EVs) derived from *L. crispatus* PMC201.

GO-term	description	count in network	strength	false discovery rate
GO:0005576	Extracellular region	8 of 29	0.91	0.0014
GO:0009274	Peptidoglycan-based cell wall	4 of 12	0.99	0.0263
GO:0005618	Cell wall	5 of 14	1.02	0.0122
GO:0030115	S-layer	3 of 3	1.47	0.0145

3.5.2. Analysis of Biological Processes and KEGG Pathways in Proteins from EVs Derived from *L. crispatus* PMC201

Gene Ontology (GO) analysis was performed to profile protein compositions of EVs and identify key biological processes associated with their cargo (Figure 6A, Table 5). EVs derived from *L. crispatus* PMC201 proteins were enriched in metabolic processes, emphasizing the significant role of EVs in mediating metabolic activity. EVs derived from *L. crispatus* PMC201 proteins showed significantly higher counts and strengths in glycolytic process (9 of 11, strength: 1.38) and gluconeogenesis (4 of 7, strength: 1.23). They also showed higher counts and strengths in the pyruvate metabolic process (10 of 12, strength: 1.39). Proteins extracted from EVs derived from *L. crispatus* PMC201 displayed pathways associated with carbohydrate metabolism, amino acid biosynthesis, and microbial metabolism. EVs derived from *L. crispatus* PMC201 proteins also showed a higher prevalence of pathways related to biosynthesis of primary and secondary metabolites, such as biosynthesis of secondary metabolites (20 of 100, strength: 0.71) and carbon metabolism (17 of 38, strength: 1.06) (Figure 6B, Table 6).

Preprints.org (www.preprints.org) | NOT PEER-REVIEWED | Posted: 13 May 2024 doi:10.20944/preprints202405.0897.v1

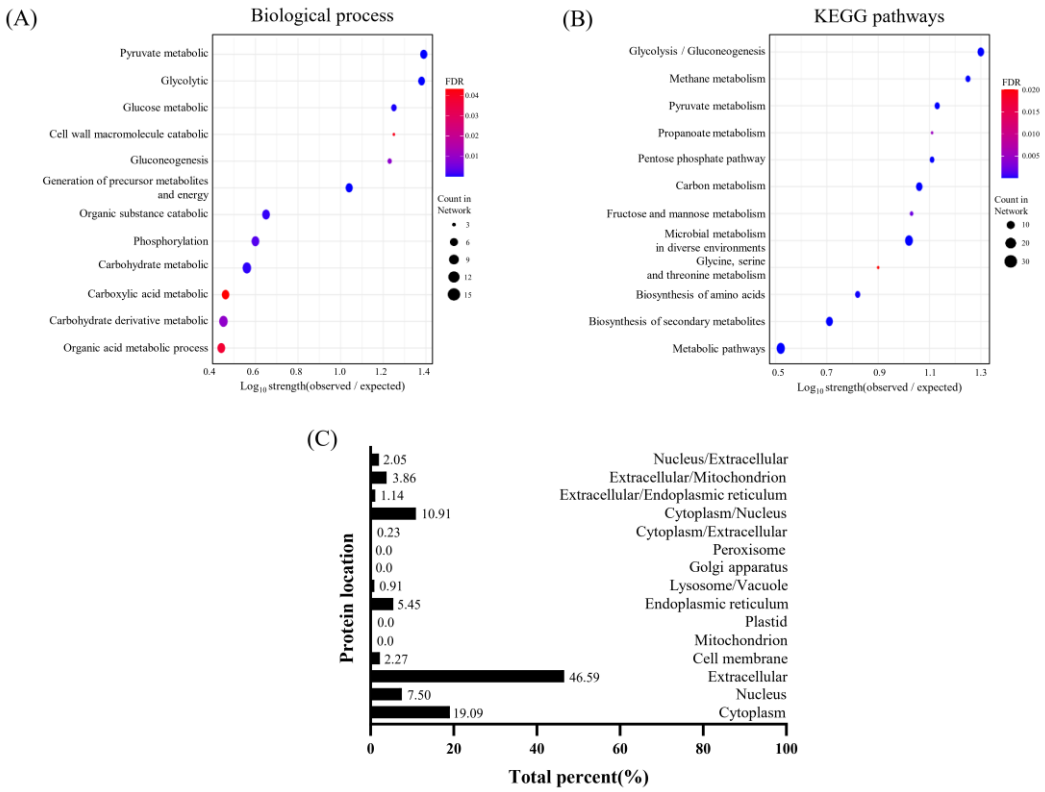

Figure 6. Prediction of protein pathways and localization. The majority of proteins in total EVs derived from *L. crispatus* PMC 201 are located in the extracellular region. (A) Biological Processes, (B) KEGG Pathways analyses pertain to proteins from EVs derived from *L. crispatus* PMC 201. (C) Predicted localization of proteins from EVs derived from *L. crispatus* PMC 201. (PPI enrichment p-value $<1.0 \times 10^{-16}$, FDR ≤ 0.05).

Table 5. Biological process of proteins from extracellular vesicles (EVs) derived from *L. crispatus* PMC201.

GO-term	description	count in network	strength	false discovery rate
GO:0006082	Organic acid metabolic process	12 of 128	0.44	0.0358
GO:1901135	Carbohydrate derivative metabolic process	15 of 159	0.45	0.0088
GO:0019752	Carboxylic acid metabolic process	11 of 113	0.46	0.0413
GO:0005975	Carbohydrate metabolic process	15 of 121	0.56	0.00074
GO:0016310	Phosphorylation	12 of 90	0.6	0.0027
GO:1901575	Organic substance catabolic process	12 of 80	0.65	0.001
GO:0006091	Generation of precursor metabolites and energy	10 of 27	1.04	8.09E-06
GO:0006094	Gluconeogenesis	4 of 7	1.23	0.0085
GO:0006006	Glucose metabolic process	6 of 10	1.25	0.00027
GO:0016998	Cell wall macromolecule catabolic process	3 of 5	1.25	0.0393
GO:0006096	Glycolytic process	9 of 11	1.38	1.33E-06
GO:0006090	Pyruvate metabolic process	10 of 12	1.39	2.85E-07

 doi:10.20944/preprints202405.0897.v1

Table 6. Kegg pathways of proteins from extracellular vesicles (EVs) derived from *L. crispatus* PMC201.

Pathway	description	count in network	strength	false discovery rate
lcr01100	Metabolic pathways	31 of 240	0.52	2.42E-08
lcr01110	Biosynthesis of secondary metabolites	20 of 100	0.71	6.37E-08
lcr01230	Biosynthesis of amino acids	10 of 39	0.82	6.75E-05
lcr00260	Glycine, serine and threonine metabolism	4 of 13	0.9	0.0201
lcr01120	Microbial metabolism in diverse environments	27 of 66	1.02	6.09E-17
lcr00051	Fructose and mannose metabolism	5 of 12	1.03	0.0023
lcr01200	Carbon metabolism	17 of 38	1.06	5.45E-11
lcr00030	Pentose phosphate pathway	8 of 16	1.11	1.22E-05
lcr00640	Propanoate metabolism	4 of 8	1.11	0.0052
lcr00620	Pyruvate metabolism	10 of 19	1.13	4.05E-07
lcr00680	Methane metabolism	9 of 13	1.25	4.05E-07
lcr00010	Glycolysis / Gluconeogenesis	18 of 23	1.3	1.10E-14

3.5.3. Investigation into Subcellular Localization of Proteins EVs Derived from *L. crispatus* PMC201

A substantial fraction of proteins within EVs derived from *L. crispatus* PMC201, amounting to 46.59%, predominantly localized to the extracellular compartment, with an additional 19.09% exhibiting a distinct presence within the cytoplasm. These results demonstrate the significant participation of EVs derived from *L. crispatus* PMC201 in extracellular matrix dynamics, underscoring their significance in intercellular signaling and tissue homeostasis (Figure 6C).

3.5.4. Protein Interactions within EVs Derived from *L. crispatus* PMC201

Interactions among proteins identified in EVs derived from *L. crispatus* PMC201 revealed a network primarily centered around large ribosomal subunit protein, glyceraldehyde-3-phosphate dehydrogenase(gap), enolase (eno), glucose-6-phosphate isomerase (pgi), phosphoglycerate kinase (pgk), and L-lactate dehydrogenase (ldh) (Figure 7A). These proteins, when considered as the core, are associated with essential biological processes such as pyruvate metabolic process, glycolytic process, generation of precursor metabolites and energy, and organic acid metabolic process.

 doi:10.20944/preprints202405.0897.v1

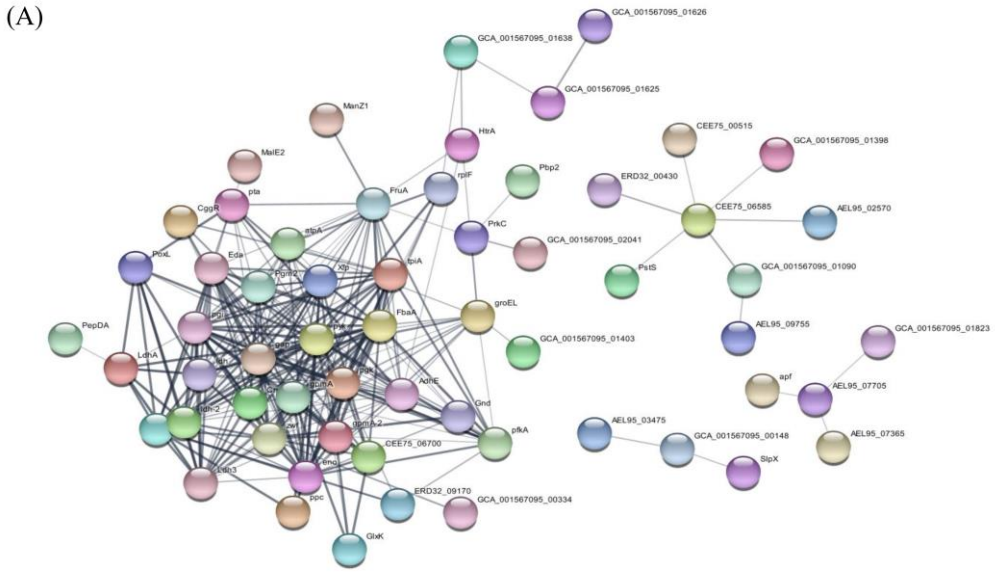

Figure 7. Interaction network of proteins from extracellular vesicles (EVs) derived *L. crispatus* PMC201. Protein interactions within EVs of *L. crispatus* PMC201 are depicted. These interactions reveal complex molecular networks underlying the functionality of bacterial EVs.

4. Discussion

EVs derived from ***L. crispatus*** PMC201 strain and the proteome they possess were investigated in this study. While EVs derived from probiotic bacteria are significant, proteomic studies on isolated EVs are also being conducted. However, there is a shortage of reports regarding functional characteristics and mechanisms of action of probiotic EVs and proteomes [27]. The function of EVs varies not only depending on the type and origin of bacteria, but also on the quantity of EVs themselves and conditions of bacteria and their culture methods [28]. Therefore, we used food-grade media [24] instead of conventional MRS media. The secretion of EVs particles was more effectively achieved with the food-grade media than with the MRS media. EVs derived from *Lactobacillus* spp. were associated with immune responses. Treatment with EVs derived from *L. plantarum* can inhibit the secretion of major inflammatory cytokines and increase the secretion of the anti-inflammatory cytokine IL-10 without causing tissue damage [29]. Additionally, attention has been paid to EVs because they have been found to help drug delivery across the blood-brain barrier (BBB) using both passive and active targeting strategies, promote gene therapy for targeted tissues, and deliver chemotherapy drugs to tumors [30]. These characteristics suggest the possibility of targeting the lungs, which are involved in tuberculosis, for therapeutic purposes. *M.tuberculosis* is recognized by the C-type lectin pattern recognition receptor (PRR) DC-SIGN (dendritic cell-specific intercellular adhesion molecule 3-capture nonintegrin) [31,32]. DC-SIGN is a transmembrane protein with a C-type calcium-dependent lectin, which can capture antigens for processing and presentation of a viral and bacterial nature. Viruses (such as HIV-1, Ebola, Juniper, and dengue fever) and important bacteria such as *M. tuberculosis* have previously been shown to be recognized by lectins [33,34,35]. Among many *Lactobacillus* species reported as probiotics, several possess S-layer proteins that exhibit an antiviral activity against herpesvirus-2 [36]. The S layer of *Lactobacillus acidophilus* has been demonstrated to possess a protective antiviral effect against Junín virus, an important human pathogen, by blocking virus entry into host cells through the DC-SIGN receptor [37]. Based on these findings, it is conceivable that the S-layer protein of ***L. crispatus*** PMC201 might influence the interaction between *M.tuberculosis* and DC-SIGN, potentially resulting in an anti-tuberculosis effect. When efficacies of specific proteins derived from bacterial EVs are examined, it has been found that glycerol-3-phosphate dehydrogenase (GAPDH) secreted from *L. reuteri* BBC3 vesicles can reduce intestinal inflammation damage induced by lipopolysaccharides (LPS) [38]. Lipoteichoic acid of *L.*

 doi:10.20944/preprints202405.0897.v1

paracasei D3-5 cell walls can enhance mucin (Muc2) expression and reduce intestinal inflammation by regulating the TLR-2/p38-MAPK/NF-kB pathway [39]. Additionally, GAPDH secreted from *L. plantarum* EVs has been found to have anti-inflammatory effects against *Staphylococcus aureus* infection and ability to bind to human colonic mucus [40]. The function of each protein within EVs can be noted and the mechanism of action can be understood through studies on interactions of found proteins. GAPDH, one of the most abundant proteins in *L. crispatus* PMC201, has previously been proven to be present in *L. plantarum* EVs with anti-inflammatory effects [40]. It might have an efficacy in treating tuberculosis. Proteins of EVs derived from *L. crispatus* PMC201 included S-layer, GADPH, and various other proteins such as peptidoglycan-binding protein, N-acetyl muramidase, beta-lactamase family protein, and enolase. Studies on the mechanisms of action and interactions of EVs or proteins from lactic acid bacteria strains are still lacking. Their effects as tuberculosis therapeutics have not been revealed yet. If we look at the efficacy and mechanism of action of each protein, we can predict that we will be able to find a protein that has potential as an adjuvant for tuberculosis treatment. Therefore, further studies are needed to identify characteristics of proteins, find proteins with immunomodulatory mechanisms related to tuberculosis treatment, and identify protein combinations that can induce synergistic effects.

5. Conclusions

This is a follow-up study of *Lactobacillus crispatus* PMC201, a strain with anti-tuberculosis activity. EVs derived from this strain were confirmed. In addition, experiments were conducted on medium compositions and isolation methods to effectively isolate EVs. This paper optimized culture conditions for characterization and isolation of EVs derived from *L. crispatus* PMC201, showing yield differences when *L. crispatus* PMC201 was cultured in commercial media MRS and food-grade media. Food-grade media secreted about 2.5 times more EVs, allowing for more efficient EV isolation. In addition, since the particle number was higher when EVs were isolated by UC than by SEC method, proteomic analysis was performed using food-grade media and UC method. A total of 64 proteins were identified in EVs derived from *L. crispatus* PMC 201, with s-layer proteins showing the highest abundance. Identified proteins were mainly located in the extracellular space. The analysis confirmed biological processes and protein-protein interactions of proteins identified in EVs derived from *L. crispatus* PMC 201. In conclusion, our study confirmed that strain *L. crispatus* PMC201 with anti-tuberculosis efficacy secreted EVs and found a medium that could obtain a high yield of its EVs. We further found that this method was effective for purifying EVs from probiotics, isolating EVs from anti-TB strains, and optimizing culture conditions for therapeutic development. This method could also produce therapeutics for other important bacterial pathogens.

Author Contributions: Conceptualization, data curation, formal analysis, Software, Validation, Visualization, Writing - original draft, Soyeon Lee.; Writing - review & editing, Soyeon Lee and Youngkyoung Lee.; Investigation, methodology, Soyeon Lee, Youngkyoung Lee and Haekang Yang.; Project Administration, Supervision, Dongsic Choi; Funding acquisition, Hoonhee Seo and Ho-yeon Song. All authors have read and agreed to the published version of the manuscript.

Funding: This research was supported by the National Research Foundation of Korea's Leading Research Center project (RS-2023-00219563) under the Ministry of Science and ICT. This work was also supported by the Technology Innovation Program (20018499) supported by the Korean Ministry of Trade, Industry, and Energy (MOTIE, Korea). Additionally, this research was supported by the Soonchunhyang University Research Fund.

Data Availability Statement: The raw data supporting the conclusions of this article will be made available by the authors on request.

Conflicts of Interest: The authors declare no conflicts of interest.

 doi:10.20944/preprints202405.0897.v1

References

1. FAO/WHO, "Health and Nutritional Properties of Probiotics in Food including Powder Milk with Live Lactic Acid Bacteria," Oct. 2001.
2. FDA, "Scientific Evaluation of the Evidence on the Beneficial Physiological Effects of Isolated or Synthetic Non-Digestible Carbohydrates Submitted as a Citizen Petition (21 CFR 10.30): Guidance for Industry." [Online]. Available: http://www.regulations.gov.
3. M. Kechagia et al., "Health Benefits of Probiotics: A Review," ISRN Nutr, vol. 2013, pp. 1–7, Jan. 2013, doi: 10.5402/2013/481651.
4. Z. Li et al., "Chemically and Biologically Engineered Bacteria-Based Delivery Systems for Emerging Diagnosis and Advanced Therapy," *Advanced Materials*, vol. 33, no. 38. John Wiley and Sons Inc, Sep. 01, 2021. doi: 10.1002/adma.202102580.
5. B. Chugh and A. Kamal-Eldin, "Bioactive compounds produced by probiotics in food products," *Current Opinion in Food Science*, vol. 32. Elsevier Ltd, pp. 76–82, Apr. 01, 2020. doi: 10.1016/j.cofs.2020.02.003.
6. L. G. Ruiz Rodríguez et al., "Diversity and functional properties of lactic acid bacteria isolated from wild fruits and flowers present in northern Argentina," *Front Microbiology*, vol. 10, no. MAY, 2019, doi: 10.3389/fmicb.2019.01091.
7. A. Raheem, L. Liang, G. Zhang, and S. Cui, "Modulatory Effects of Probiotics During Pathogenic Infections with Emphasis on Immune Regulation," *Frontiers in Immunology*, vol. 12. Frontiers Media S.A., Apr. 08, 2021. doi: 10.3389/fimmu.2021.616713.
8. M. Bermudez-Brito, J. Plaza-Díaz, S. Muñoz-Quezada, C. Gómez-Llorente, and A. Gil, "Probiotic mechanisms of action," *Annals of Nutrition and Metabolism*, vol. 61, no. 2. pp. 160–174, Oct. 2012. doi: 10.1159/000342079.
9. M. Cunningham et al., "Shaping the Future of Probiotics and Prebiotics," *Trends in Microbiology*, vol. 29, no. 8. Elsevier Ltd, pp. 667–685, Aug. 01, 2021. doi: 10.1016/j.tim.2021.01.003.
10. K. S. Yoha, S. Nida, S. Dutta, J. A. Moses, and C. Anandharamakrishnan, "Targeted Delivery of Probiotics: Perspectives on Research and Commercialization," *Probiotics and Antimicrobial Proteins*, vol. 14, no. 1. Springer, pp. 15–48, Feb. 01, 2022. doi: 10.1007/s12602-021-09791-7.
11. S. Lin et al., "Surface-modified bacteria: synthesis, functionalization and biomedical applications," Chemical Society Reviews, vol. 52, no. 19. Royal Society of Chemistry, pp. 6617–6643, Sep. 19, 2023. doi: 10.1039/d3cs00369h.
12. M. Liu, J. Chen, I. P. W. Dharmasiddhi, S. Chen, Y. Liu, and H. Liu, "Review of the Potential of Probiotics in Disease Treatment: *Mechanisms, Engineering, and Applications*," Processes, vol. 12, no. 2. Multidisciplinary Digital Publishing Institute (MDPI), Feb. 01, 2024. doi: 10.3390/pr12020316.
13. P. Krzyżek, B. Marinacci, I. Vitale, and R. Grande, "Extracellular Vesicles of Probiotics: Shedding Light on the Biological Activity and Future Applications," *Pharmaceutics*, vol. 15, no. 2. MDPI, Feb. 01, 2023. doi: 10.3390/pharmaceutics15020522.
14. N. Díaz-Garrido, J. Badia, and L. Baldomà, "Microbiota-derived extracellular vesicles in interkingdom communication in the gut," *Journal of Extracellular Vesicles*, vol. 10, no. 13. John Wiley and Sons Inc, Nov. 01, 2021. doi: 10.1002/jev2.12161.
15. J. A. Molina-Tijeras, J. Gálvez, and M. E. Rodríguez-Cabezas, "The immunomodulatory properties of extracellular vesicles derived from probiotics: A novel approach for the management of gastrointestinal diseases," *Nutrients*, vol. 11, no. 5. MDPI AG, May 01, 2019. doi: 10.3390/nu11051038.
16. R. M. Stubbendieck, C. Vargas-Bautista, and P. D. Straight, "Bacterial communities: Interactions to scale," *Frontiers in Microbiology*, vol. 7, no. AUG. *Frontiers in Microbiology* S.A., Aug. 08, 2016. doi: 10.3389/fmicb.2016.01234.
17. S. Domingues and K. M. Nielsen, "Membrane vesicles and horizontal gene transfer in prokaryotes," *Current Opinion in Microbiology*, vol. 38, pp. 16–21, Aug. 2017, doi: 10.1016/J.MIB.2017.03.012.
18. N. Díaz-Garrido, J. Badia, and L. Baldomà, "Microbiota-derived extracellular vesicles in interkingdom communication in the gut," *Journal of Extracellular Vesicles*, vol. 10, no. 13. John Wiley and Sons Inc, Nov. 01, 2021. doi: 10.1002/jev2.12161.
19. C. Mu, Y. Yang, and W. Zhu, "Crosstalk between the Immune Receptors and Gut Microbiota," *Current Protein & Peptide Science,* Volume 16, Issue 7, pp. 622-632, 2015, doi 10.2174/1389203716666150630134356

20. B. Thay, A. Damm, T. A. Kufer, S. N. Wai, and J. Oscarsson, "*Aggregatibacter* actinomycetemcomitans outer membrane vesicles are internalized in human host cells and trigger NOD1- and NOD2-dependent NF-κB activation," *Infection and Immunity*, vol. 82, no. 10, pp. 4034–4046, 2014, doi: 10.1128/IAI.01980-14.
21. M. Chatzidaki-Livanis, M. J. Coyne, and L. E. Comstock, "An antimicrobial protein of the gut symbiont Bacteroides fragilis with a MACPF domain of host immune proteins," *Molecular Microbiology*, vol. 94, no. 6, pp. 1361–1374, Dec. 2014, doi: 10.1111/mmi.12839.
22. R. A. ñahui Palomino, S. Zicari, C. Vanpouille, B. Vitali, and L. Margolis, "Vaginal *lactobacillus* inhibits HIV-1 replication in human tissues ex vivo," *Frontiers in Microbiology*, vol. 8, no. MAY, May 2017, doi: 10.3389/fmicb.2017.00906.
23. Y. Lee et al., "Activity of *Lactobacillus crispatus* isolated from vaginal microbiota against Mycobacterium tuberculosis," *Journal of Microbiology*, vol. 59, no. 11, pp. 1019–1030, 2021, doi: 10.1007/s12275-021-1332-0.
24. H. Tajdozian, Y. kyoung Lee, S. Kim, Y. Kyoung Jeong, and S. Kwak Kyung Chungnam Techno Park Jung-Hyun Ju, "Ecacy of lyophilized *Lactobacillus sakei* as a potential candidate for the prevention of carbapenem-resistant Klebsiella infection," *Research square*, 2023, doi: 10.21203/rs.3.rs-2834556/v1.
25. J. Lee et al., "Proteomic analysis of extracellular vesicles derived from *Mycobacterium tuberculosis*," *Proteomics*, vol. 15, no. 19, pp. 3331–3337, Oct. 2015, doi: 10.1002/pmic.201500037.
26. D. Choi et al., "Quantitative proteomics and biological activity of extracellular vesicles engineered to express SARS-CoV-2 spike protein," *Journal of Extracellular Biology*, vol. 1, no. 10, Oct. 2022, doi: 10.1002/jex2.58.
27. C. Bäuerl, J. M. Coll-Marqués, C. Tarazona-González, and G. Pérez-Martínez, "*Lactobacillus casei* extracellular vesicles stimulate EGFR pathway likely due to the presence of proteins P40 and P75 bound to their surface," *Scientific Reports*, vol. 10, no. 1, Dec. 2020, doi: 10.1038/s41598-020-75930-9.
28. J. Kowal et al., "Proteomic comparison defines novel markers to characterize heterogeneous populations of extracellular vesicle subtypes," *Proceedings of the National Academy of Sciences*, vol. 113, no. 8, pp. E968–E977, Feb. 2016, doi: 10.1073/pnas.1521230113.
29. W. Kim et al., "*Lactobacillus plantarum*-derived extracellular vesicles induce anti-inflammatory M2 macrophage polarization in vitro," *Journal of Extracell Vesicles*, vol. 9, no. 1, Jan. 2020, doi: 10.1080/20013078.2020.1793514.
30. J. Ren, W. He, L. Zheng, and H. Duan, "From structures to functions: Insights into exosomes as promising drug delivery vehicles," *Biomaterials Science*, vol. 4, no. 6. Royal Society of Chemistry, pp. 910–921, Jun. 01, 2016. doi: 10.1039/c5bm00583c.
31. T. B. H. Geijtenbeek et al., "Mycobacteria target DC-SIGN to suppress dendritic cell function," *Journal of Experimental Medicine*, vol. 197, no. 1, pp. 7–17, Jan. 2003, doi: 10.1084/jem.20021229.
32. L. Tallieux et al., "DC-SIGN is the major *Mycobacterium tuberculosis* receptor on human dendritic cells," *Journal of Experimental Medicine*, vol. 197, no. 1, pp. 121–127, Jan. 2003, doi: 10.1084/jem.20021468.
33. M. G. Martinez, M. A. Bialecki, S. Belouzard, S. M. Cordo, N. A. Candurra, and G. R. Whittaker, "Utilization of human DC-SIGN and L-SIGN for entry and infection of host cells by the New World arenavirus, Junín virus," *Biochemical and Biophysical Research Communications*, vol. 441, no. 3, pp. 612–617, Nov. 2013, doi: 10.1016/j.bbrc.2013.10.106.
34. E. A. Koppel, K. P. J. M. van Gisbergen, T. B. H. Geijtenbeek, and Y. van Kooyk, "Distinct functions of DC-SIGN and its homologues L-SIGN (DC-SIGNR) and mSIGNR1 in pathogen recognition and immune regulation," *Cellular Microbiology*, vol. 7, no. 2. pp. 157–165, Feb. 2005. doi: 10.1111/j.1462-5822.2004.00480.x.
35. P. Konieczna et al., "*Bifidobacterium infantis* 35624 administration induces Foxp3 T regulatory cells in human peripheral blood: Potential role for myeloid and plasmacytoid dendritic cells," *Gut Microbes*, vol. 61, no. 3, pp. 354–366, Mar. 2012, doi: 10.1136/gutjnl-2011-300936.
36. P. Mastromarino, F. Cacciotti, A. Masci, and L. Mosca, "Antiviral activity of *Lactobacillus brevis* towards herpes simplex virus type 2: Role of cell wall associated components," *Anaerobe*, vol. 17, no. 6, pp. 334–336, Dec. 2011, doi: 10.1016/j.anaerobe.2011.04.022.
37. M. G. Martínez, M. Prado Acosta, N. A. Candurra, and S. M. Ruzal, "S-layer proteins of *Lactobacillus acidophilus* inhibits JUNV infection," *Biochemical and Biophysical Research Communications*, vol. 422, no. 4, pp. 590–595, Jun. 2012, doi: 10.1016/j.bbrc.2012.05.031.
38. R. Hu et al., "*Lactobacillus reuteri*-derived extracellular vesicles maintain intestinal immune homeostasis against lipopolysaccharide-induced inflammatory responses in broilers," *Journal of Animal Science and Biotechnology*, vol. 12, no. 1, Dec. 2021, doi: 10.1186/s40104-020-00532-4.

 doi:10.20944/preprints202405.0897.v1

39. S. Wang et al., "Lipoteichoic acid from the cell wall of a heat killed *Lactobacillus paracasei* D3-5 ameliorates aging-related leaky gut, inflammation and improves physical and cognitive functions: from C. elegans to mice," *Geroscience*, vol. 42, no. 1, pp. 333–352, Feb. 2020, doi: 10.1007/s11357-019-00137-4.
40. J. S. Ong et al., "Extracellular transglycosylase and glyceraldehyde-3-phosphate dehydrogenase attributed to the anti-staphylococcal activity of *Lactobacillus plantarum* USM8613," *Journal of Biotechnology*, vol. 300, pp. 20–31, Jul. 2019, doi: 10.1016/j.jbiotec.2019.05.006.